Radial Hele-Shaw flow with suction: Fully nonlinear pattern formation

Ching-Yao Chen* and Yu-Sheng Huang
Department of Mechanical Engineering, National Chiao Tung University, Hsinchu, Taiwan, 30010 Republic of China

José A. Miranda†
Departamento de Física, Universidade Federal de Pernambuco, Recife, Pernambuco 50670-901 Brazil
(Received 15 January 2014; published 9 May 2014)

We study the development of intricate, fully nonlinear immiscible interfacial patterns in the suction-driven radial Hele-Shaw problem. The complex-shaped, contracting fluid-fluid interface arises when an initially circular blob of more viscous fluid, surrounded by less viscous one, is drawn into an eccentric point sink. We present sophisticated numerical simulations, based on a diffuse interface model, that capture the most prominent interfacial features revealed by existing experimental studies of the problem. The response of the system to changes in the capillary number is investigated, accurately revealing the occurrence of finger competition phenomena, and correctly describing the velocity behavior of both inward- and outward-pointing fingers. For the large-capillary-number regime, a set of complex interfacial features (finger merging, shielding, and pinch-off) whose experimental realization is still not available, are predicted.

DOI: 10.1103/PhysRevE.89.053006 PACS number(s): 47.15.gp, 47.54.−r, 47.51.+a, 47.11.−j

I. INTRODUCTION

The viscous fingering problem [1] is one of the most studied among fluid dynamic systems presenting formation and evolution of elaborate patterned structures. It considers the development of interfacial instabilities when a fluid displaces another of higher viscosity between the narrowly spaced plates of a Hele-Shaw cell [2]. A very popular, and intensively investigated, version of the problem is the so-called radial fingering flow driven by injection. It considers the radial invasion of a less viscous fluid that is injected under a constant injection rate against a more viscous liquid that initially occupies the whole cell. The injection is performed through an inlet located at the center of the upper cell plate. Experiments involving the injection-driven radial flow for immiscible fluids demonstrate that as the size of the fluid-fluid interface grows outward, fingers form, spread, and start to split at their tips, creating complex branched patterns [3–9]. Numerical investigations [10–12] used boundary integral and conformal mapping techniques to accurately reproduce the pattern-forming structures observed in such experiments.

A closely related problem to the conventional injection-driven, immiscible flow in radial Hele-Shaw geometry results if a blob of a more viscous fluid, surrounded by a less viscous fluid, is sucked and drawn radially inward into a sink located at the center of the cell. This setup defines the suction-driven radial Hele-Shaw flow. This version of the problem has been treated analytically in the zero surface tension limit via conformal mapping methods. In this context, the main interest of both theoretical physicists and applied mathematicians was mostly in examining a finite-time blow-up of the interfacial solutions, as well as cusp formation phenomena [13–15]. Boundary integral simulations have also been utilized to investigate the interface behavior for the small, finite-surface-tension situation [16–18]. It has been found that the zero surface tension cusp formation is avoided, and instead a narrow finger of the less viscous fluid forms, which then rapidly propagates towards the sink. It is worth noticing that all these works focused on understanding the regularizing effects of surface tension and not exactly on the precise morphological description of the interfacial patterns at advanced time stages.

In contrast to the radial Hele-Shaw problem driven by injection, the analysis of fully nonlinear patterns induced by suction for arbitrary, finite surface tension through experiments and numerical simulations has been largely unexploited. On the experimental side, there are just a couple of studies, which were performed sometime ago [3,8]. The authors of Refs. [3,8] focused on the situation of maximum viscosity contrast, where the surrounded fluid has negligible viscosity. These experimental works have revealed the development of patterns that markedly differ from those traditionally obtained in injection-driven flows (see Fig. 10 in Ref. [3] and Fig. 15 in Ref. [8]). During the suction of the more viscous inner fluid it has been observed that the initially circular fluid-fluid interface shrinks and deforms by the penetration of multiple fingers of the less viscous outer fluid. The invading fingers compete, and eventually a single finger reaches the sink, while the remaining fingers basically stop their inward moving growth. It has also been noticed that under suction the penetrating fingers do not tend to split at their tips, so instead of finger tip-splitting the most prevalent pattern-forming mechanism is indeed finger competition.

With respect to numerical simulations of the fully nonlinear pattern formation dynamics under suction, only a few studies have been undertaken: in Refs. [19–21] for the quarter five-spot configuration and in Ref. [22] for the usual radial Hele-Shaw setup. However, differently from the immiscible flow circumstances experimentally examined in Refs. [3,8], these studies [19–22] consider that the fluids involved are miscible. Therefore, a numerical investigation of the advanced time pattern-forming phenomena occurring under suction of immiscible fluids in radial Hele-Shaw cells still needs to be performed. This is in fact the main purpose of our current paper. In this work we apply a diffuse interface formalism

*chingyao@mail.nctu.edu.tw
†jme@df.ufpe.br

[23,24] to the suction-driven radial Hele-Shaw flow. First, we try to reproduce as accurately as possible the main morphological aspects of the patterns experimentally obtained in Refs. [3,8]. Then we explore and predict other important morphological features that have not yet been unveiled by laboratory experiments.

The rest of this paper is organized in three additional sections. Section II is devoted to introduce the setup of the physical problem, the application of the diffuse interface formalism to the suction-driven radial Hele-Shaw flow, and the related governing equations. Section III presents our numerical results, revealing a number of relevant interfacial structures as capillary effects are varied. The occurrence of finger pinch-off and droplet entrapment phenomena are discussed. Our main conclusions are presented in Sec. IV.

II. PHYSICAL PROBLEM AND GOVERNING EQUATIONS

Consider a Hele-Shaw cell of constant gap thickness h containing two immiscible, incompressible, viscous fluids (see Fig. 1). Denote the viscosities of the fluids, respectively, as η_2 (inner fluid) and η_1 (outer fluid) and assume that $\eta_2 > \eta_1$. Initially, the fluid-fluid interface is a circle of diameter D_0, and a Cartesian coordinate system (x,y,z) is defined in such a way that its origin is located at the center of this circular region. The inner fluid is sucked at a point sink located at the center, and the suction process continues up to a time $t = t_f$, when the area of the inner fluid reduces to $\pi {D_f}^2/4$. This suction scheme is performed at a constant flow rate Q, equal to the area covered per unit time, and given by $Q = \pi({D_0}^2 - {D_f}^2)/4t_f$. Driven by the action of suction, as time progresses the interface becomes unstable, giving rise to complex interfacial shapes.

The governing equations for a diffuse interface description of the problem, which is based on a Boussinesq Hele-Shaw-Cahn-Hilliard model [23,24], can be written as

$$\nabla \cdot \mathbf{u} = 0, \tag{1}$$

$$\nabla p = -\frac{12\eta}{h^2}\mathbf{u} - \epsilon\rho\nabla\cdot[(\nabla c)(\nabla c)^T], \tag{2}$$

$$\rho\left(\frac{\partial c}{\partial t} + \mathbf{u}\cdot\nabla c\right) = \alpha\nabla^2\mu, \tag{3}$$

$$\mu = \frac{\partial f_0}{\partial c} - \epsilon\nabla^2 c. \tag{4}$$

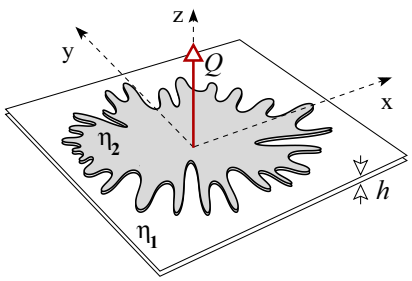

FIG. 1. (Color online) Sketch of a suction-driven radial flow in a Hele-Shaw cell of constant gap width h. The more viscous fluid of viscosity η_2 ($\eta_2 > \eta_1$) is sucked at the center of the cell [origin of the (x,y,z) coordinate system] with constant flow rate Q. As a consequence, complex interfacial patterns arise.

Here, $\mathbf{u}$, p, η, and ρ successively denote the velocity vector, the pressure, the viscosity, and the density of the binary fluid system. In the context of our current problem the density ρ is assumed to be constant. The phase-field variables of the inner and outer fluids are set as $c = 0$ and $c = 1$, respectively. The constant ϵ represents the coefficient of capillarity, while the constant α denotes the coefficient of mobility. The chemical potential is μ, and f_0 is the classical part of the free energy (or the Helmholtz free energy). To simulate an immiscible interface, a convex profile of the Helmholtz free energy with a characteristic specific energy f^*, e.g., $f_0 = c^2(1-c)^2 f^*$, is applied. The above expressions result in a surface free energy E given by

$$E = \rho\int\left[f_0 + \frac{\epsilon}{2}(\nabla c)^2\right]dV, \tag{5}$$

where V is the volume of the fluid domain. In this framework, the viscosity η is assumed to be related to the phase-field variable c as [20,25,26]

$$\eta(c) = \eta_1 e^{[R(1-c)]},\ R = \ln\left(\frac{\eta_2}{\eta_1}\right). \tag{6}$$

In order to render the governing equations and relevant variables dimensionless, D_0 and t_f are taken as the characteristic scales. This leads to a characteristic suction rate ${D_0}^2/t_f$. Furthermore, the pressure is scaled by $(12\eta_1 D_0^2)/(t_f h^2)$. Thus, the dimensionless version of the governing equations is

$$\nabla\cdot\mathbf{u} = 0, \tag{7}$$

$$\nabla p = -\eta\mathbf{u} - \frac{C}{S}\nabla\cdot\left[(\nabla c)(\nabla c)^T\right], \tag{8}$$

$$\frac{\partial c}{\partial t} + \mathbf{u}\cdot\nabla c = \frac{1}{\mathrm{Pe}}\nabla^2\mu, \tag{9}$$

$$\mu = \frac{\partial f_0}{\partial c} - C\nabla^2 c, \tag{10}$$

$$f_0 = c^2(1-c)^2, \tag{11}$$

$$Q = \frac{\pi}{4}(1 - {D_c}^2). \tag{12}$$

Dimensionless parameters, such as the viscosity contrast A, the Péclet number Pe, the Cahn number C, the suction strength S, and the terminal core diameter D_c, are defined as

$$\mathrm{Pe} = \frac{\rho D_0^2}{\alpha f^* t_f},\ A = \frac{e^R - 1}{e^R + 1},\ C = \frac{\epsilon}{D_0^2 f^*},$$

$$S = \frac{12\eta_1 D_0^2}{\rho f^* h^2 t_f},\ D_c = \frac{D_f}{D_0}.$$

The diffusional Péclet number and the Cahn number are the nondimensional measures of the dissipation and dispersion in the model [27]. $\mathrm{Pe} \sim O(1/\gamma)$ and $C \sim O(\gamma^2)$, where γ measures the interface thickness, are proposed in Ref. [23].

Another important dimensionless parameter in the context of injection- and suction-driven flows in radial Hele-Shaw flows is the capillary number, which can be defined as the ratio of the driven pressure by the suction, i.e., characteristic

pressure $(12\eta_1 {D_0}^2)/(h^2 t_f)$, and the surface pressure $\tilde{\sigma}/D_0$, and can be defined as [28]

$$\widetilde{\mathrm{Ca}} = \frac{12\eta_1 D_0}{\tilde{\sigma} t_f}\left(\frac{D_0}{h}\right)^2, \tag{13}$$

where $\tilde{\sigma}$ stands for the surface tension. Within the diffuse interface formulation, if a one-dimensional interface (associated with a given spatial variable ζ) is assumed, a dimensionless equilibrium surface tension (or free energy) can be expressed as [29]

$$\sigma = \frac{1}{\mathrm{S}}\int\left[f_0 + \frac{C}{2}\left(\frac{\partial c}{\partial \zeta}\right)^2\right]d\zeta. \tag{14}$$

The equilibrium surface tension σ can be calculated theoretically to replace the surface tension $\tilde{\sigma}$ appearing in Eq. (13), so an equilibrium capillary number takes the form [24]

$$\mathrm{Ca} = \frac{3S}{\sqrt{C/2}}. \tag{15}$$

The numerical methods we employ in this work are similar to the ones develop in Refs. [20,22,24,25], in which the governing equations are recast into the well-known stream function (ϕ)-vorticity (ω) formulation, yielding

$$u = \frac{\partial \phi}{\partial y},\ v = -\frac{\partial \phi}{\partial x}, \tag{16}$$

$$\nabla^2 \phi = -\omega, \tag{17}$$

where

$$\omega = -R\left(u\frac{\partial c}{\partial y} - v\frac{\partial c}{\partial x}\right) + \frac{C}{\eta S}\left[\frac{\partial c}{\partial x}\left(\frac{\partial^3 c}{\partial x^2 \partial y} + \frac{\partial^3 c}{\partial y^3}\right) - \frac{\partial c}{\partial y}\left(\frac{\partial^3 c}{\partial x \partial y^2} + \frac{\partial^3 c}{\partial x^3}\right)\right].$$

In the present radial Hele-Shaw flow, the rotational part of the velocity is smooth and can be obtained with high accuracy, while the potential part of the inward velocity induced by suction is related to a flow singularity at a sink. The flow singularity makes accurate computations more difficult near these locations. To avoid numerical instabilities near the sink, we smooth out the point sink by distributing its strength in a Gaussian way over a small circular core region. To accomplish this, we consider a "Gaussian sink" [20,22,25] which is characterized by a core size $D_c = 0.15$. The magnitude of the dimensionless potential radial velocity satisfying these requirements can be expressed as

$$\mathbf{u}_{\mathrm{pot}} = -\frac{Q}{2\pi r}[1 - \exp(-4r^2/{D_c}^2)]\hat{\mathbf{r}}, \tag{18}$$

where r denotes the radial distance away from the point sink and $\hat{\mathbf{r}}$ represents the unit vector along the radial direction.

Our simulations are carried in a square computational domain with length of 4/3. An initial circular more viscous blob is placed at the center of the domain, so the interface is located at $r = 0.5$. The simulations are terminated when the penetrating less viscous fluid reaches the Gaussian core at $r = 0.075$. This is done to minimize the effect of the core on the simulations. Moreover, boundary conditions are prescribed as follows:

$$x = \pm 2/3 : \phi = 0,\ \frac{\partial c}{\partial x} = 0,\ \frac{\partial^2 c}{\partial x^2} = 0, \tag{19}$$

$$y = \pm 2/3 :\ \phi = 0,\ \frac{\partial c}{\partial y} = 0,\ \frac{\partial^2 c}{\partial y^2} = 0. \tag{20}$$

Since the flux across the boundary is prescribed by the potential part, the rotational components of velocity are confined in the computational domain. As a result, the vanishing stream function can be applied on the boundary. Moreover, since the drop shrinks inward, the phase-field variable is uniform on the boundaries, so zero values of gradients and second derivatives are used.

To reproduce the extremely fine structures of the fingers, a highly accurate pseudospectral method is employed. As a result, the actual boundary conditions applied in the numerical code are $\partial\phi/\partial x = 0$ at $x = \pm 2/3$. However, at the present situation where no gradient of the phase variable is generated on the boundaries, the above conditions automatically lead to $\phi = 0$. Both c and ϕ are expanded in a cosine series in the x direction. In the y direction, discretization is accomplished by sixth-order compact finite differences. Time integration is fully explicit and utilizes a third-order Runge-Kutta procedure. The evaluation of the nonlinearity at each time level is performed in a pseudospectral manner.

It should be noted that the mixed compact finite difference–spectral method implemented for the Poisson equation is identical to the scheme applied in miscible fluid simulations [26], which is a modification of the purely spectral approach [20,25]. While the miscible simulations performed by using the purely spectral approach [20,25] were validated by comparing the growth rates with the respective values obtained from linear stability theory, comparable accuracy of the mixed method to the purely spectral approach was confirmed in a different class of flows [30]. In addition, the validations of the mixed method incorporated with the immiscible simulations are supported by the good qualitative agreement with respect to pattern formation, and good quantitative agreement for the number of fingers, which had been achieved in the early work of rotational flows [24] as well as in suction flows presented below. Nevertheless, similarly to the conventional finite difference method, numerical instability might occur if the gradient of phase-field variable within the diffuse interface is too significant. For a more detailed account about these numerical schemes and their validations, the reader is referred to Refs. [20,24–26,30].

III. NUMERICAL RESULTS AND DISCUSSION

In this section we focus on displaying numerical simulations associated with significantly high viscosity contrast, where the fingering instability is more prominent. So, throughout this work we present a series of simulations for a fixed value of the viscosity contrast, namely $A = 0.922$. This is the maximum possible value of A we were able to simulate for all range of Ca we study in this work, by keeping our numerical code stable. In fact, this is the closest we can get of the situation that has been experimentally investigated in Refs. [3,8], where $A = 1$. Moreover, following Ref. [24], we

consider that Pe $= 10^3$, and $C = 10^{-5}$ in all the simulations. However, the capillary number Ca [given by Eq. (15)] is allowed to vary in order to evaluate the relative effects of suction and surface tension, and their influence on the pattern formation process.

Before we proceed, a few comments about the chosen value for the Cahn number are in order. It is known that variation of the Cahn number C changes the thickness of the interface, so larger values of C can lead to strong diffusion through the interface [31]. Therefore, to properly reach the sharp interface limit one should consider a sufficiently small Cahn number. On the other hand, the use of a Cahn number that is too small could result in numerical instability. In this work, in order to ensure the numerical stability of our code for all values of the capillary number Ca we study, we utilize a fixed small value of the Cahn number given by $C = 10^{-5}$. The appropriateness of this particular value of C is indirectly validated by the good qualitative agreement between simulated and experimental patterns, as well as quantitative predictions regarding the number of fingers, which had been achieved in our previous work on rotating Hele-Shaw flows [24], and also on the suction-driven flows displayed here.

Figure 2 presents simulated patterned structures for three values of the capillary number Ca = 1342, 2683, and 5367, taken at time $t = 0.65$ and at the breakthrough time t_b. The breakthrough time is defined when a dominant finger of the inner less viscous fluid reaches the position of the Gaussian core ($r = D_c/2$). The breakthrough times for these three cases are $t_b = 0.834$, 0.752, and 0.684, respectively. In all cases an initially circular interface destabilizes due to the Saffman-Taylor instability, and at early times a large number of fingers develop. As time advances the penetrating fingers of the less viscous fluid move inward, and their amplitudes grow. These penetrating fingers present different sizes, clearly indicating that there exists a competition among them as they move toward the sink. Large length variability of the invading fingers means larger competition. At later times, it can be noticed that a smaller fraction of the inward pointing fingers actually are able to "win the race" toward the center. We have also observed that the fingers which have been left behind are screened off, and their velocities are significant reduced. Then, at $t = t_b$, we see that a longer winning finger, closely accompanied by other competing fingers, reaches the Gaussian core near the center of the Hele-Shaw cell.

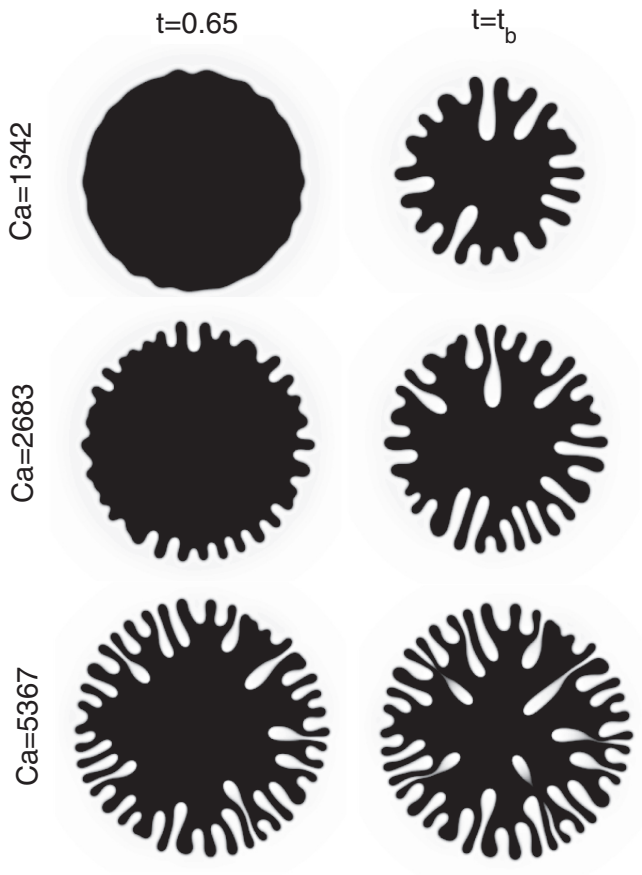

FIG. 2. Numerical simulations showing typical fingering patterns at times $t = 0.65$, and the breakthrough time t_b, for increasingly larger values of the capillary number: Ca = 1342 ($t_b = 0.834$), Ca = 2683 ($t_b = 0.752$), and Ca = 5367 ($t_b = 0.684$).

Although the general aspects of the simulated patterns depicted in Fig. 2 are qualitatively in line with the ones experimentally detected for inward radial flows with immiscible fluids [3,8], the agreement between their specific morphological features is not perfect. For instance, while the experiment presented in Ref. [8] (see, for instance, their Fig. 15) shows that one single finger ends up breaking through, the simulated structures illustrated in Fig. 2 indicate that a few dominant fingers can arise and compete in the race to the sink point. We believe this is in part due to the fact that the immiscible experiments in Ref. [8] are performed for the maximum viscosity contrast case $A = 1$, while the simulations shown in Fig. 2 consider that $A = 0.922$. The value of A is crucial in determining the actual number of dominant fingers. We point out that a similar behavior has also been observed in experiments [32,33] and simulations [34] for immiscible flows in rectangular Hele-Shaw cells, where the presence of a single dominant finger is clearly detected when $A = 1$, but not when $A < 1$ where a larger number of fingers can compete as front runners. In addition, it is possible that the fact that we imposed an artificial Gaussian sink [Eq. (18)], for which true breakthrough of the dominant fingers cannot be simulated, could also contribute to create differences between simulations and experiments with respect to the specific competition among dominant fingers at later times.

The numerical simulations shown in Fig. 2 are reassuring in the sense that they are able to capture the most salient dynamic and morphological aspects of the experiments. Additional information can been extracted from our numerical results shown in Fig. 2: It is apparent that by increasing the capillary number Ca more vigorous fingering is detected. In this cases, one observes a larger number of resulting fingers, and smaller values of the breakthrough times. These numerical results make perfect sense and serve to reinforce the validity and effectiveness of our diffuse interface method.

We continue by discussing other relevant aspects of the fingering patterns illustrated in Fig. 2. One of the most conspicuous behaviors is related to the phenomenon of finger competition, which refers to finger length variability.

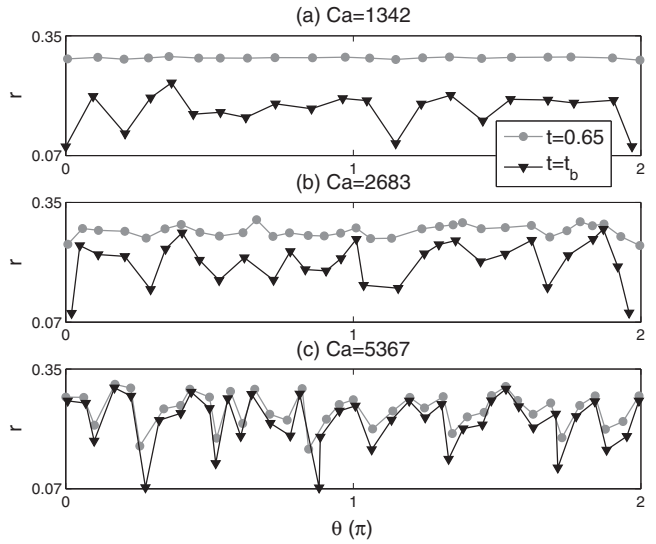

FIG. 3. Finger competition behavior for the patterns illustrated in Fig. 2 for (a) Ca = 1342, (b) Ca = 2683, and (c) Ca = 5367. The radial positions of the fingertips of inward fingers r are plotted as a function of the polar angle θ. Clearly, the number of fingers, and the competition among them are larger for higher values of the capillary number.

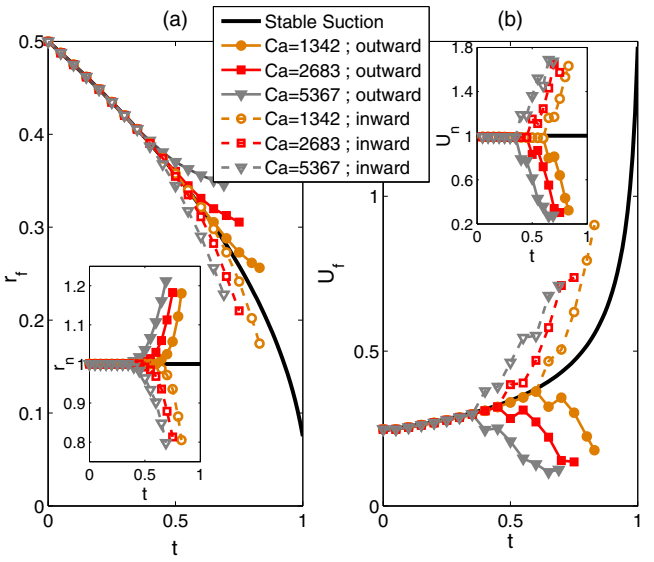

FIG. 4. (Color online) A more quantitative display of important dynamic features of the patterns shown in Fig. 2: (a) Averaged fingertip positions (r_f) of inward and outward fingers with time; (b) averaged radial speeds (U_f) of inward and outward fingers as time is varied. The insets show normalized values of positions (r_n) and velocities (U_n) which are scaled by the instantaneous values related to the suction of a stable circular fluid-fluid interface (solid black curve). The normalized averaged positions and radial speeds of the inward and outward fingertips are quite symmetric, which reflects faster inward fingers associated with slowly moving outward fingers.

Throughout our analysis, we define the inward (outward) pointing fingers of the less (more) viscous fluid as *inward* (*outward*) fingers. By inspecting Fig. 2 we can see that the radial positions of the tips of the outward fingers form a nearly circular interface which slowly contracts as time advances. This indicates that the competition among outward fingers is not very intense. At the same time, one can verify the quick penetration of the inward fingers, whose fingertips are located at clearly distinct radial positions. This shows the evident finger competition among rapidly moving inward fingers. These numerical findings are also consistent with the general dynamical features revealed by experiments [3,8].

The competition among inward fingers can be even more clearly observed in Fig. 3, which plots the radial position of the tips of inward fingers as a function of polar angle θ for the situations depicted in Fig. 2. In the case of a lower value of the capillary number [Fig. 3(a)], radial positions of all the fingertips are still quite uniform at time $t = 0.65$ due to strong constraints imposed by surface tension. As suction continues, a few dominant fingers evolve, and three of them approach the Gaussian core. These dominant inward fingers are more easily identified for the cases of higher values of the capillary number [Figs. 3(b) and 3(c)]. Notice that the fingers that are left behind are shielded and remain almost stationary, while the winning fingers move quite rapidly toward the sink. Actually, these competition and shielding effects play an important role regarding the highly nonlinear merging phenomena we will discuss later in this work.

By examining Figs. 2 and 3 one can tell that the inward fingers move significantly faster than the outward fingers. A more quantitative account of this fact is shown in Fig. 4: Figure 4(a) plots the averaged radial positions r_f of the fingertips (of both inward and outward fingers) with respect time, while Fig. 4(b) depicts how the averaged radial speed of these fingers U_f evolves in time. The corresponding values for the condition of a stable suction of an unperturbed circular interface (solid black curves) are also shown. The insets show normalized values of positions (r_n) and velocities (U_n) which are scaled by the instantaneous values associated to the stable suction situation.

From Fig. 4(a) we see that as time progresses the positions of outward fingertips start to lag behind the curve of stable suction, while the fingertips of inward fingers move ahead of it. Note that more significant deviations from the stable suction case occur for higher values of the capillary number. In the inset of Fig. 4(a) it can be noticed that the movements of the inward and outward fingers appear quite symmetric when represented in terms of the normalized measurements. Even more interesting is the fact all the breakthroughs occur at times when deviations of the normalized radial positions approach about 20%, i.e., at $r_n = 0.8$ and 1.2 for the inward and outward fingers, respectively.

Similar kind of conclusions can be extracted from Fig. 4(b), where larger velocity deviations as compared to the stable suction case are observed for higher capillary numbers. Again, suggestive similarities for the breakthrough times exist, which all occur at 70% deviations, i.e., U_n=1.7 and 0.3 for the inward and outward fingers, respectively. These facts indicate that the averaged lengths of inward and outward fingers grow by nearly a same rate if the reference frame moves along with the stable suction interface.

The fact that the fingers that do not grow fast compared to the dominant ones are slowed down can be explained

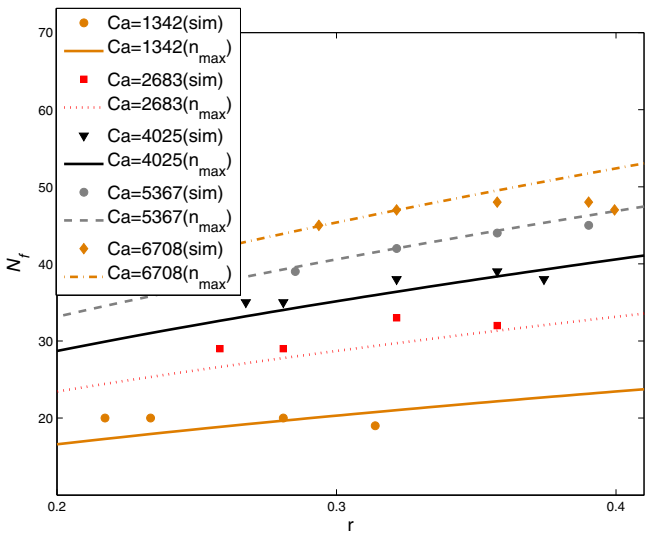

FIG. 5. (Color online) Variation of the number of fingers N_f with the radial distance r to the shrinking perturbed interface for different values of the capillary number Ca. Corresponding analytical predictions for the number of fingers ($n_{\max}$) as given by Eq. (22) are also shown. Good general agreement is obtained.

physically through the fingering phenomenon of shielding (see, e.g., the article by Homsy in Ref. [2]). Shielding can be understood as the tendency of a finger to grow in the direction of the pressure gradient. As the fingers grow inwards, the available space is more and more restricted and their growth is hindered. In this scenario, the longer fingers grow faster and obstruct the growth of the shorter fingers in their vicinities. This shielding effect is similar to what is commonly seen in experiments and simulations of rectangular Hele-Shaw flows [32–34] where shielding is very effective when $A = 1$ and is progressively less intense as the viscosity contrast is decreased ($A < 1$). In addition, since the velocity field is inversely proportional to the radial distance [Eq. (18)], the variation of local velocity would enhance the different advancing speeds among the fingers. Once the fingers are ahead, the faster inward velocity drives the fingers further ahead of the slower fingers.

Another quantitative measurement of relevance is related to the number of interfacial fingers. Figure 5 illustrates that the number of penetrating inward fingers N_f, obtained from our numerical simulations (sim), varies with the radial distance to the evolving interface r for different values of the capillary number Ca. As demonstrated by the representative evolutions shown in Fig. 2, numerous interface ripples start to grow after a given latent period, so it is difficult to determine the precise number of fingers at shorter times, before significant growth has set in. Therefore, the extraction of N_f from the simulations involves some uncertainties. Having said this, we stress that the numbers recorded in Fig. 5 are counted only after individual fingers can be clearly identified. In this setting, the number of fingers increases slightly after the first measurement and then might remain nearly constant (e.g., Ca = 1342) or decrease continuously (e.g., Ca = 5367). As expected, a higher value of the capillary number is always associated with a larger number of fingers. These numerical results for N_f can be directly compared to early time linear stability predictions for the number of interfacial fingers. At the linear level, the number of fingers is connected to the maximum of the growth rate and given (in dimensional form) as [3,35]

$$n_{\max}(r) = \sqrt{\frac{1}{3}\left(1 + \frac{AQ}{2\pi\alpha}r\right)}, \tag{21}$$

where

$$\alpha = \frac{h^2\sigma}{12(\eta_1 + \eta_2)}.$$

After proper rescaling, and assuming that

$$Q = \frac{\pi({D_0}^2 - {D_c}^2)}{4t_f} \approx \frac{\pi {D_0}^2}{4t_f},$$

$$\eta_2 - \eta_1 = (e^R - 1)\eta_1 \approx e^R\eta_1,$$

a dimensionless version for Eq. (21) can be written as

$$n_{\max}(r) \approx \sqrt{\frac{1}{3}\left(1 + \frac{e^R \mathrm{Ca}}{8}r\right)}. \tag{22}$$

This expression is used to plot the analytical prediction curves shown in Fig. 5. General good agreement is obtained between analytical ($n_{\max}$) and numerical (sim) predictions for the number of fingers. This good agreement provides additional validation for our numerical simulations.

At first glance, the good match between the results of our fully nonlinear simulations and those given by Eq. (22), originally obtained in Ref. [35], may seem surprising. After all, Eq. (22) has been derived by a linear stability calculation and, hence, should not normally extend beyond the early linear regime. This is particularly true for the injection-driven Hele-Shaw case [1–12], where the nonlinear phenomena of finger tip-splitting is vividly present, resulting in finger branching and finger proliferation. Of course, this introduces significant discrepancies between linear predictions and the actual number of measured fingers in more advanced stages of the dynamics. However, for suction-driven Hele-Shaw flows the emerging inward moving fingers do not split, so finger tip-splitting events are absent [3,8]. Because of this fact, fingers do not proliferate in the suction flow case, so the linear predictions are not as bad when one compares linear data with the actual number of fingers detected at nonlinear stages of the dynamics. Finally, we point out that a similar good agreement between linear and nonlinear predictions for the number of interfacial fingers can also been found in the rotating Hele-Shaw problem, where finger tip-splitting phenomena are also not present [36].

Possible reasons for the existing mismatch between N_f and $n_{\max}$ as shown in Fig. 5 could be the occurrence of fully nonlinear phenomena, for instance, finger merging, which can alter the counting of the inward fingers at advanced times. Of course, these nonlinear effects are not taken into account by the linear stability calculation leading to $n_{\max}$.

Up to this point we have concentrated our discussion on the qualitative comparison of our numerical patterns (Fig. 2) with those detected by a few available laboratory experiments [3,8]. In doing so, we used typical capillary number values similar to those utilized in Refs. [3,8]. As a result, we managed to obtain interfacial structures that resemble the experimental ones. In

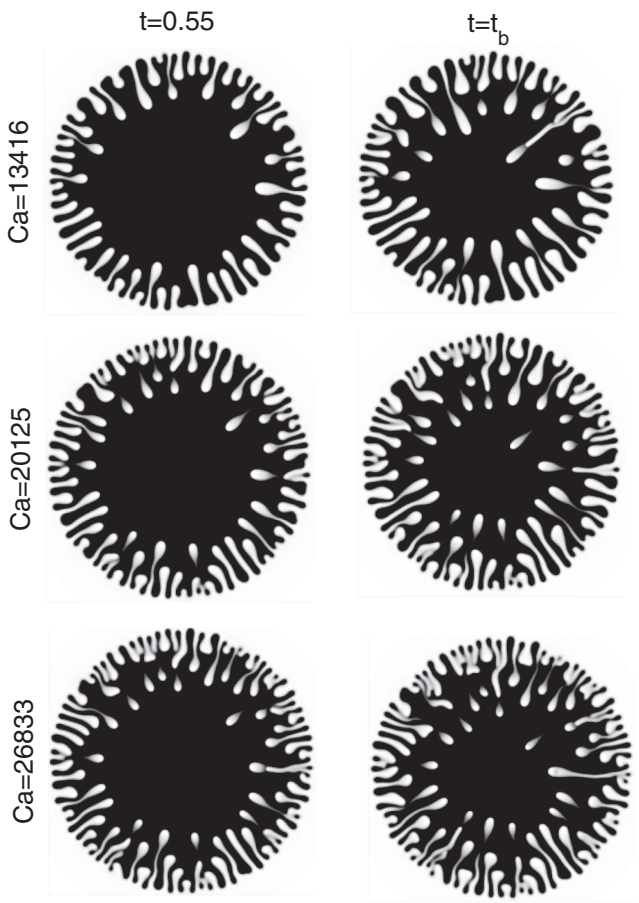

FIG. 6. Typical fingering patterns in the limit of high capillary numbers Ca and for $A = 0.922$, exhibiting prominent nonlinear phenomena such as finger merging, shielding, and pinch-off at time $t = 0.55$ and at the breakthrough time t_b: (a) Ca = 13461 ($t_b = 0.608$), (b) Ca = 20125 ($t_b = 0.598$), and (c) Ca = 26833 ($t_b = 0.589$).

addition, our numerical model was also able to capture the main dynamic features revealed by experiments, namely the finger competition phenomena, as well as the velocity behavior of both inward and outward fingers. To close this work, we want to predict morphological characteristics and dynamic behaviors that have not yet being assessed by experiments. One way to perform such analysis is to run simulations for higher values of the capillary number Ca. This is done in Fig. 6 for Ca = 13416, 20125, and 26833. We stress that the high capillary numbers used in Fig. 6 are indeed realistic. For actual Hele-Shaw experiments using very high capillary numbers (5.0×10^4), please see, for instance, Maxworthy's work published in Ref. [37]. So, for example, if one uses a more viscous fluid (e.g., a mineral oil) of viscosity 0.03 Pa s, surface tension 5–50 mN/m, $D_0/h \sim 100$, and operating time $t_f < 5$ s, the corresponding capillary number would be in the range used in Ref. [37].

The numerical simulations for the high capillary number limit shown in Fig. 6 do unveil dynamical and morphological behaviors that have not yet been observed by experiments of suction-driven flows in radial Hele-Shaw cells. In this high-Ca regime, a considerably large number of inward fingers penetrate the initially circular, more viscous blob so fingering is really intense. This leads to the production of quite convoluted patterned structures. In all cases depicted in Fig. 6 we see that multiple inward fingers compete: Some quickly advance toward the sink, while the growth of others is shielded. The first noteworthy fact is the observation that some fingers merge while they move. Interestingly, as a result of this finger-merging process, the roots of the dominant (or winning) fingers are squeezed and eventually pinch-off, forming encapsulated, island drops of the less-viscous fingers inside the more-viscous one. Simultaneously, one also observes the pinch-off of the slow-moving outward fingers of the more viscous fluid that have been left behind. Consequently, tiny satellite droplets of the more viscous fluid arise at the rim of the patterned structures. It is also evident that the formation of both entrapped and satellite drops are favored for larger values of the capillary number. One advantageous aspect of our diffuse interface model (as opposed to usual sharp interface numerical methods) is the fact that we can predict and contemplate the formation of such interesting merging and pinch-off events.

We point out that the occurrence of finger merging and pinch-off had been actually observed in numerical simulations of radial Hele-shaw flows involving miscible fluids [22,38], where the effects of surface tension are negligible. However, they are not very commonly discussed in injection- or suction-driven radial Hele-Shaw displacements when the confined fluids are immiscible. This is true despite the fact that pinch-off and merging phenomena have indeed been observed in experiments [39] and simulations [40] of immiscible fluids in rectangular Hele-Shaw geometry. The appearance of pinch-off and satellite drops under immiscible circumstances have also been detected by experiments [36] and by phase-field [41] and diffuse interface [24] simulations for radial flow in rotating Hele-Shaw cells. Finally, the pinching-off of droplets from the main body of the more viscous fluid has also been unfolded in lifting Hele-Shaw flows, both by numerical simulations with miscible fluids [42], as well as by experiments with immiscible fluids [43]. So the shielding, merging, and pinch-off of fingers detected numerically in Fig. 6 sounds quite plausible, and we hope experimentalists will feel motivated to obtain them in the laboratory.

By inspecting Fig. 6 it is evident that the resulting fingering structures become very thin for very large values of Ca. This might cause concerns on the validity of Hele-Shaw assumption, where the gap width needs to be smallest length scale of the problem. In the present study, the gap width is embedded in the dimensionless suction strength S and does not appear in the formulation explicitly. As a result, the validity of the model can be ensured by properly combining the relevant control parameters with a sufficiently small gap width. In this context, the general validity of the model is kept even when fingers are very thin. Nevertheless, one should be cautious when interpreting the results when they are converted back to the dimensional description. In this case, the limitation of Hele-Shaw assumption has to be carefully checked.

We close this section by commenting on the lack of a more quantitative parallel between our numerical results and the experiments presented in Refs. [3] and [8]. Unfortunately, these studies [3,8] do not allow for a more quantitative comparison between our numerical results and their experiments.

For example, Ref. [8] discusses the suction flow case very qualitatively: This is done in a single paragraph (see p. 238 of Ref. [8], in a section entitled "Convergent flow"), and only one picture of the experiment is provided (see p. 239 of Ref. [8], their Fig. 15). No specific experimental data, such as the time evolution of the number of fingers is presented, so not much can be extracted other than the shape of the resulting pattern. Moreover, in their Fig. 15 no scale bar is provided. The same type of remarks can be made with respect to the experiment displayed in Ref. [3]: Again, the discussion of the suction flow situation is very brief (see pp. 523–526 of Ref. [3] in a section entitled "Inward Fingering"), and just a photograph of the experiment is shown (see p. 525 of Ref. [3], their Fig. 10, where there is no scale bar). Similarly to that presented in Ref. [8], no quantitative, systematic experimental data involving the pattern evolution can be assessed. These observations justify why a more quantitative comparison between our numerical results and the available experiments [3,8] could not be done. Of course, this indicates that even on the purely experimental side, much still needs to be done regarding suction flow in Hele-Shaw cells.

IV. CONCLUSION

We have performed intensive numerical simulations in order to probe the advanced time pattern formation dynamics of the radial viscous fingering problem induced by suction. By employing a diffuse interface model we have been able to generate complex patterns which contain the most important morphological and dynamic features detected by previous experimental investigations of the problem. In agreement with experimental observations we have identified patterns showing a strong competition among inward pointing fingers, while outward pointing fingers do not compete as much. Our numerical predictions regarding the velocity of both inward and outward fingers, as well as the ones describing the number of fingers that evolve with time, are also in line with experiments and linear stability calculations, respectively. All these conclusions have been reached for a set of values for the capillary number. Moreover, at the large capillary number regime we unveiled some interesting phenomena that have not yet being analyzed experimentally, namely the occurrence of characteristic finger-merging and pinch-off events. In this scenario, we predicted the possible uprising of both entrapped island drops of the less viscous fluid and of satellite droplets of the more viscous fluid located at peripheral regions of the patterns.

ACKNOWLEDGMENTS

J.A.M. thanks CNPq for financial support through the program "Instituto Nacional de Ciência e Tecnologia de Fluidos Complexos (INCT-FCx)" and FACEPE through PRONEM Project No. APQ-1415-1.05/10. C.-Y.C. thanks the National Science Council of the Republic of China for financial support through Grant No. NSC 101-2221-E-009-033-MY3.

[1] P. G. Saffman and G. I. Taylor, Proc. R. Soc. London Ser. A **245**, 312 (1958).
[2] G. M. Homsy, Annu. Rev. Fluid Mech. **19**, 271 (1987); K. V. McCloud and J. V. Maher, Phys. Rep. **260**, 139 (1995); J. Casademunt, Chaos **14**, 809 (2004).
[3] L. Paterson, J. Fluid Mech. **113**, 513 (1981).
[4] S. N. Rauseo, P. D. Barnes, and J. V. Maher, Phys. Rev. A **35**, 1245 (1987).
[5] S. E. May and J. V. Maher, Phys. Rev. A **40**, 1723 (1989).
[6] J. D. Chen, Exp. Fluids **5**, 363 (1987).
[7] J. D. Chen, J. Fluid Mech. **201**, 223 (1989).
[8] H. Thomé, M. Rabaud, V. Hakim, and Y. Couder, Phys. Fluids A **1**, 224 (1989).
[9] O. Praud and H. L. Swinney, Phys. Rev. E **72**, 011406 (2005).
[10] P. Fast and M. J. Shelley, J. Comput. Phys. **212**, 1 (2006).
[11] J. Mathiesen, I. Procaccia, H. L. Swinney, and M. Thrasher, Eur. Phys. Lett. **76**, 256 (2006).
[12] S. W. Li, J. S. Lowengrub, J. Fontana, and P. Palffy-Muhoray, Phys. Rev. Lett. **102**, 174501 (2009).
[13] S. Richardson, J. Fluid Mech. **102**, 263 (1981).
[14] Y. E. Hohlov and S. D. Howison, Q. Appl. Math. **51**, 777 (1993).
[15] L. J. Cummings and J. R. King, Eur. J. Appl. Math. **15**, 1 (2004).
[16] E. D. Kelly and E. J. Hinch, Eur. J. Appl. Math. **8**, 533 (1997).
[17] H. D. Ceniceros, T. Y. Hou, and H. Si, Phys. Fluids **11**, 2471 (1999).
[18] H. D. Ceniceros and H. Si, J. Comput. Phys. **165**, 237 (2000).
[19] P. Philippe, C.-Y. Chen, E. Meiburg, and T. Maxworthy, Phys. Fluids **11**, 1705 (1999).
[20] C.-Y. Chen and E. Meiburg, J. Fluid Mech. **371**, 233 (1998).
[21] C.-Y. Chen and E. Meiburg, J. Fluid Mech. **371**, 269 (1998).
[22] C.-Y. Chen, C.-W. Huang, H. Gadêlha, and J. A. Miranda, Phys. Rev. E **78**, 016306 (2008).
[23] H.-G. Lee, J. S. Lowengrub, and J. Goodman, Phys. Fluids **14**, 492 (2002).
[24] C.-Y. Chen, Y.-S. Huang, and J. A. Miranda, Phys. Rev. E **84**, 046302 (2011).
[25] E. Meiburg and C.-Y. Chen, SPE J. **5**, 129 (2000).
[26] M. Ruith and E. Meiburg, J. Fluid Mech. **420**, 225 (2000).
[27] J. Lowengrub and L. Truskinovsky, Proc. R. Soc. London Ser. A **454**, 2617 (1998).
[28] E. O. Dias, E. Alvarez-Lacalle, M. S. Carvalho, and J. A. Miranda, Phys. Rev. Lett. **109**, 144502 (2012).
[29] P. T. Yue, J. J. Feng, C. Liu, and J. Shen, J. Fluid Mech. **515**, 293 (2004).
[30] C. Härtel, E. Meiburg, and F. Necker, J. Fluid Mech. **418**, 189 (2000).
[31] C. F. Zhou, P. T. Yue, J. J. Feng, C. F. Ollivier-Gooch, and H. H. Hu, J. Comput. Phys. **229**, 498 (2010).
[32] J. V. Maher, Phys. Rev. Lett. **54**, 1498 (1985).
[33] M. W. DiFrancesco and J. V. Maher, Phys. Rev. A **39**, 4709 (1989); **40**, 295 (1989).
[34] G. Tryggvason and H. Aref, J. Fluid Mech. **154**, 287 (1985).
[35] J. A. Miranda and M. Widom, Physica D **120**, 315 (1998).
[36] E. Alvarez-Lacalle, J. Ortín, and J. Casademunt, Phys. Fluids **16**, 908 (2004).
[37] T. Maxworthy, J. Fluid Mech. **177**, 207 (1987).
[38] C.-Y. Chen, C.-W. Huang, L.-C. Wang, and J. A. Miranda, Phys. Rev. E **82**, 056308 (2010).

[39] M. G. Moore, A. Juel, J. M. Burgess, W. D. McCormick, and H. L. Swinney, *Proceedings of the Seventh Experimental Chaos Conference*, edited by I. Visarath, L. Kocarev, T. L. Carroll, B. J. Gluckman, S. Boccaletti, and J. Kurths, Vol. 676 (Springer-Verlag, Berlin, 2003), pp. 189–194.

[40] G. Tryggvason and H. Aref, J. Fluid Mech. **136**, 1 (1983).

[41] R. Folch, E. Alvarez-Lacalle, J. Ortín, and J. Casademunt, Phys. Rev. E **80**, 056305 (2009).

[42] C.-Y. Chen, C.-H. Chen, and J. A. Miranda, Phys. Rev. E **71**, 056304 (2005).

[43] A. Lindner, D. Derks, and M. J. Shelley, Phys. Fluids **17**, 072107 (2005).